CHIN. PHYS. LETT. Vol. 38, No. 4 (2021) 045203

Energetic Particle Transport Prediction for CFETR Steady State Scenario Based on Critical Gradient Model

Yunpeng Zou(邹云鹏)[1], V. S. Chan(陈锡熊)[2,3], Wei Chen(陈伟)[1*], Yongqin Wang(王雍钦)[1], Yumei Hou(侯玉梅)[1], and Yiren Zhu(朱毅仁)[1]

[1]*Southwestern Institute of Physics, Chengdu 610041, China*
[2]*General Atomics, San Diego, CA 92186, USA*
[3]*School of Nuclear Science and Technology, University of Science and Technology of China, Hefei 230026, China*

(Received 1 December 2020; accepted 2 February 2021; published online 6 April 2021)

The critical gradient mode (CGM) is employed to predict the energetic particle (EP) transport induced by the Alfvén eigenmode (AE). To improve the model, the normalized critical density gradient is set as an inverse proportional function of energetic particle density; consequently, the threshold evolves during EP transport. Moreover, in order to consider the EP orbit loss mechanism in CGM, ORBIT code is employed to calculate the EP loss cone in phase space. With these improvements, the AE enhances EPs radial transport, pushing the particles into the loss cone. The combination of the two mechanisms raises the lost fraction to 6.6%, which is higher than the linear superposition of the two mechanisms. However, the loss is still far lower than that observed in current experiments. Avoiding significant overlap between the AE unstable region and the loss cone is a key factor in minimizing EP loss.

DOI: 10.1088/0256-307X/38/4/045203

The China fusion engineering test reactor (CFETR)[1] is designed to be the next-generation fusion facility; one of its aims is self-sustainable burning state with a fusion gain of $Q \approx 20$–30.[2] The behavior of energetic particles (EPs), particularly α particles generated by the fusion reaction, influences heating power, bootstrap current, helium ash exhausting, etc.[3] Unfortunately, the integrated simulation based on the OMFIT framework[4] does not include an EP model for EP instability and transport estimation. Instead, in this framework, the ONETWO code[5] is employed to roughly predict the α particle's radial profile. A number of experiments[6–8] have proved that there is an obvious distinction between the classical slowing down model and realistic distribution. The primary reason for this is that Alfvén eigenmodes (AEs) driven by EP could enhance EP transport conversely, in a manner resembling a feedback system. Currently, various simulation methods, such as MEGA,[9,10] are being developed to accurately calculate EP distribution. However, due to the huge computational effort and long simulation time required, these methods are inconvenient for CFETR design. Thus, an efficient method, critical gradient model (CGM),[11] is employed to estimate α particle redistribution due to AE instabilities.

According to the current analytical theory,[12] AE is destabilized by the EP pressure gradient. Since the contribution of temperature gradient is slight[13] on threshold calculation, neglecting the effect of the temperature gradient, there should be a critical density gradient for marginal stable AE. The CGM therefore assumes that if the EP density gradient exceeds the threshold, the EP transport would be enhanced, and the diffusivity would increase significantly. The existence of the critical gradient and EP stiff transport is confirmed by the simulation[11,14] and has been experimentally verified.[15] GYRO code[16] was employed to calculate the local critical gradient, which was then input into ALPHA,[17] a 1D EP density transport code. Diffusivity was assumed to be a linear function of the distinction between EP gradient and threshold. This combination of GYRO and ALPHA was then used to estimate the EP redistribution.[18] Owing to the significant computational demands of GYRO, a parallelized wrapper, TGLFEP,[13] has been employed in its place for the purpose of efficient threshold scanning. In addition, the ALPHA code has been rewritten to EPtran[19] by expending EP distribution into $(\psi, E, v_{\|}/v)$ space. Thus, this work employs a combination of TGLFEP and EPtran to predict EP transport.

The key issue for the CGM is critical gradient calculation. Since both GYRO and TGLFEP function as local stability analysis programs, the frequency and growth rate are calculated using local plasma parameters. For each flux surface, we select AEs from multiple numerical output based on mode structure and frequency, choosing the AE with maximum growth rate to calculate the critical gradient. In previous versions of the CGM, a parameter for density gradient was used to estimate AE marginal stability. We have

Supported by the National Key R&D Program of China (Grant No. 2019TFE03020000), the National Natural Science Foundation of China (Grant Nos. 11875021, 12005054, and 12005055), the Sichuan Science and Technology Program (Grant No. 2020jqqn0070).
*Corresponding author. Email: chenw@swip.ac.cn
© 2021 Chinese Physical Society and IOP Publishing Ltd

reduced the density gradient until the AE growth rate is equal to zero, i.e., the critical density gradient is calculated to satisfy the condition of $\gamma_{\rm AE} = 0$. During the scanning process, the characteristic length of EP density $[L_{n_{\rm EP}} = -n_{\rm EP}/(dn_{\rm EP}/dr)]$ is fixed. Clearly, the assumption of fixed characteristic length means that the profile shape could not change, which is inconsistent with the reality. Although a correction factor was added,[13] the profile was modified only slightly, with an additional artificial parameter required for the correction. Instead, we select the normalized density gradient for marginal stability estimation, and the normalized critical density gradient is set as a function of EP density. To relax this assumption, we resort to an analytic formula of AE growth rate,[20]

$$\frac{\omega_{\rm i}}{k_\parallel v_{\rm A}} = -q_0^2\Big[\frac{\beta_{\rm c}}{2}(G^{\rm T}_{\rm mi}+G^{\rm T}_{\rm me}) + \beta_\alpha(G^{\rm T}_{\rm s\alpha} - nq_0\delta_\alpha H^{\rm T}_{\rm sa})\Big]. \quad (1)$$

Here, only β_α and δ_α $[\propto dp_\alpha/(p_\alpha dr)]$ will be modified during EP transport. Since the drive term includes both pressure and pressure gradient, $L_{n_{\rm EP}}$ should be allowed to vary during EP profile evolution. For marginal stability, Eq. (1) can be rewritten as

$$\frac{a}{L^{\rm th}_{n_{\rm EP}}} = \frac{k_1}{n_{\rm EP}} + k_2, \quad (2)$$

where k_1 represents the Landau damping of bulk plasma, k_2 is the Landau damping of the EP itself, and the temperature gradient drive of the EP. The TGLFEP code confirmed the inversely proportional relationship via parameter scanning (Fig. 1). The threshold calculated by TGLFEP are depicted as points, fitted by the dashed curve. Consequently, the coefficients k_1 and k_2 are obtained by the fitting curve, and then input into the transport code, EPtran. Note that the coefficients k_1 and k_2 require to be calculated for each surface. Meanwhile, the diffusivity is rewritten based on Eq. (9) in Ref. [19] as follows:

$$D^{\rm rr}_{\rm EP} = D_{\rm AE}\Big[\frac{a}{L_{n_{\rm EP}}} - \frac{a}{L^{\rm th}_{n_{\rm EP}}}\Big]_{>0} + D_{\rm ITG/TEM}, \quad (3)$$

where $[x]_{>0} = 0$ if $x < 0$.$D_{\rm AE}$ is an artificial transport coefficient, set to be large enough to drive EP transport generally. The value affects the transported profile only slightly. Here $a/L_{n_{\rm EP}}$ represents the normalized density gradient during transport, and $a/L^{\rm th}_{n_{\rm EP}}$ is the normalized critical density gradient. $D_{\rm ITG/TEM}$ denotes the micro-turbulent transport of EP obtained via the Angioni model.[21] By virtue of this improved method of threshold calculation, the threshold of each surface can be modified during EP transport.

Furthermore, the previous CGM only considered EP loss induced by diffusion at the last closed flux surface (LCFS); as a result, most of the EPs are deposited near the edge rather than being lost. Indeed, the non-uniformity of the magnetic field leads to drifts in the guiding center. Both passing particles and trapped particles may escape from the LCFS due to the wide orbit width. The behavior of the EP depends on location, energy, and pitch angle. To estimate whether or not a particle is lost, ORBIT code[22] is therefore employed to calculate the loss cone in phase space.

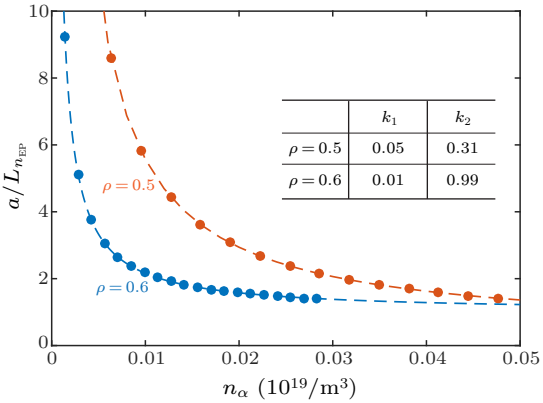

Fig. 1. Normalized critical gradient for $\rho = 0.5$ and $\rho = 0.6$ as an inverse proportional function of EP density. The TGLFEP simulation results are depicted as points, fitted by the dashed curves.

We have now established a workflow to calculate EP distribution via multiple programming methods. EFIT code[23] is employed to construct equilibrium, which is then input into the other programs. TGLFEP code calculates the threshold for AE marginal stability. The mode structure is obtained via the MHD-kinetic code, NOVA-K,[24] and amplitude is calculated using MEGA[9] for AE saturation. The structure of the perturbation is then input into ORBIT for loss cone calculation. Finally, both threshold and loss cone are read using EPtran to obtain an EP redistribution prediction.

With these optimizations of the CGM, α particle transport and redistribution is predicted for a CFETR steady-state scenario. CFETR is designed in a large size with a major radius (R) of 7.2 m, and minor radius (a) of 2.2 m. The magnetic field is $B = 6.5$ T, and the plasma current is $I = 12$ MA. The temperature and density on the axes are $T_{\rm i}(0) = 23.5$ keV, $T_{\rm e}(0) = 24.5$ keV, and $n_{\rm e}(0) = 12.5 \times 10^{19}$ m^{-3}, respectively. Reverse magnetic shear is designed [see the red dashed curve in Fig. 2(a)] so that $q(0) = 6.36$, $q_{\rm min} = 3.55$, and $q(a) = 9.33$. The isotope fraction is assumed to be $D : T = 50 : 50$, so that the initial distribution of α particles is calculated by means of the fusion reaction, via the classical slowing down model:[25]

$$F_{\rm s}(v) = \frac{S_0\tau_{\rm s}}{4\pi}\frac{H(v_\alpha - v)}{v_{\rm c}^3 + v^3}, \quad (4)$$

where S_0 is the source intensity, $\tau_{\rm s}$ is the slowing-down time, $v_{\rm c}$ is the crossover velocity, and v_α is the α particle birth speed (3.5 MeV). The stability of TAE is analyzed using NOVA-K. The unstable toroidal mode number is wide, due to large size of the device, and the $n = 6$–10 TAEs are dominant. Owing to relatively flat

q profile within $\sqrt{\psi} = 0.2$–0.8, multiple modes can be driven by a single toroidal mode number at different radial locations. The $n = 5$ continuum and mode location are depicted in Fig. 2(a), for example. Two black solid curves depict the continuum, with the TAE gap in the middle of the two curves. The red dashed curve depicts the q profile. Three $n = 5$ TAEs are distinguished by different colors, and the mode structures are shown in the insets. The two inside modes (yellow and blue) have higher growth rates than the outside mode (orange). So many unstable modes could induce significant EP transport; however, we only consider the single toroidal mode number, which is limited by the simulation method. In this way, the dominant toroidal mode number is selected for each flux surface. The stability of TAE dominates the profile of the threshold. The initial threshold profile (no transport) is depicted by the red dashed curve in Fig. 2(b), and the normalized density gradient of classical slowing down distribution is depicted by the black solid curve. In the range from $\sqrt{\psi} = 0.4$–0.8, exceeding the threshold indicates that the TAE is unstable. During the transport, the threshold increases in the core $[\sqrt{\psi} < 0.5]$ and decreases near the edge $[\sqrt{\psi} > 0.5]$.

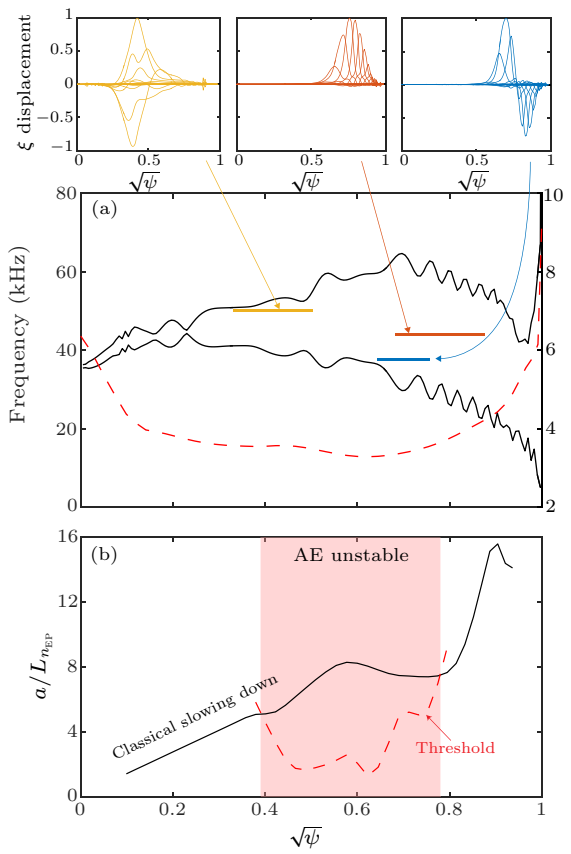

Fig. 2. (a) Shear Alfvén continuum and mode location for $n = 5$ in the TAE gap. The red dashed curve depicts the q profile. Three TAEs are depicted using different colors, and the corresponding structures are shown in the insets. (b) Threshold for α particle in CFETR steady state scenario (red dashed curve). The classical slowing-down distribution is denoted by black solid curve for comparison.

The boundary of the loss cone is depicted in Fig. 3 as a function of $\sqrt{\psi}$ and pitch angle, and the EP energy is denoted by different colors. Here, the initial EP distribution is selected to be uniform, i.e., $(\psi, E, v_\parallel/v)$, at the outer mid-plane. The simulation indicates that particles with a negative pitch angle are more easily lost, and the loss boundary peaks at $v_\parallel/v = -0.6$. The prediction of loss cone in CFETR is smaller than recent experimental values[26] due to the high magnetic field, but is slightly larger than that given by ITER,[26] since the orbital width is proportional to q. In contrast to the monotonically increasing q profile of the ITER scenario, a flat q profile with high $q_{\min}$ induces serious orbit loss. In experimental terms, the loss mechanism could be enhanced by AE perturbation, and consequently the loss cone expands. However, in the CFETR scenario, the unstable AE region and loss cone are almost separated, so that the influence of AE on the loss cone is negligible. Here, the collision between α particle and background plasma is neglected, which modifies the energy and pitch angle of the α particle in motion.

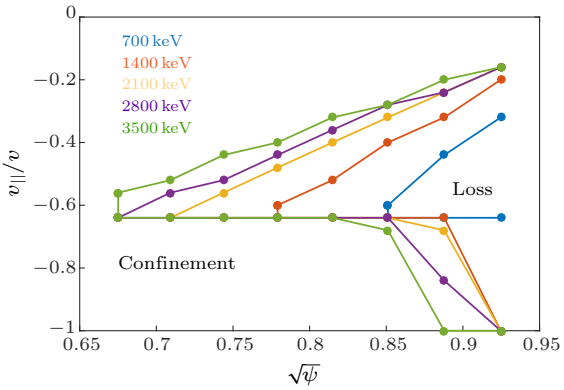

Fig. 3. The loss cone as a function of $(\psi, E, v_\parallel/v)$ for the CFETR steady-state scenario. EP energy is depicted using different colors. The points are obtained by ORBIT for loss boundary, and corresponding curves indicate linear fitting. The region on the right-hand side of the curve relates to loss, and the left-hand side refers to confinement.

The α particle deposition is denoted by a red curve in Fig. 4(a), taking into consideration both transport induced by AE, and orbit loss. For comparison, the classical slowing-down distribution is shown as a black curve, the prediction of the previous CGM is represented as a blue curve, and prediction of ONETWO is given as a purple curve, which is employed in the current OMFIT framework. The ONETWO code uses a more exact slowing down model, which includes impurity effects, the fusion reaction between beam deuterium and background tritium, and in which Coulomb collision is related to local electron density and temperature. The profiles where $\rho > 0.5$ are enlarged in the inset. The slowing down distribution is noticeably higher than the two transported profiles in the core, indicating the obvious transport of α particles subsequent to generation. Evidently, the previous CGM without FOW effect induces α parti-

cle deposition near the edge, similarly to the ITER prediction.[27] Compared with the previous CGM, the improved CGM optimizes the transport profile in the unstable AE region and edge. Moreover, in Fig. 4(b), the contribution of AE (green dash curve) and FOW (yellow dash curve) effects can be shown separately, as well as being evaluated in combination. The classical slowing down and transported profile are depicted using the same colors as those in Fig. 4(a). From the insets, we note that a high magnetic field favors a reduction in the EP loss cone, i.e., good EP confinement, so that FOW-induced loss is only 1%. AEs primarily change the shape of the EP profile, so that the loss fraction is 3.8%. In combination, unstable AEs push particles outwards into the loss cone region to enhance prompt loss, raising the loss fraction to 6.6%. Fortunately, the loss depicted by the CFETR scenario is much lower than the DIII–D discharge (50%). We attribute this to the well separation between the AE unstable region and the loss cone region.

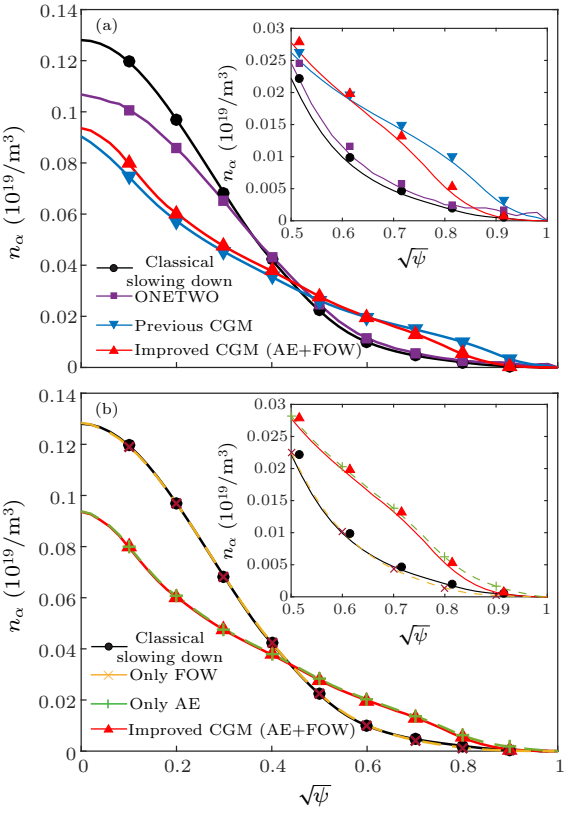

Fig. 4. (a) Behavior of α particle deposition (red curve), considering unstable AE and orbit loss. For comparison, the classical slowing-down distribution is shown as a black curve, the prediction by the previous CGM is represented by a blue curve, and the purple curve depicts the ONETWO result, which is used in current integrated simulations, based on the OMFIT framework. (b) The contribution of AE (green dashed curve) and FOW (yellow dashed curve) mechanisms are depicted separately. Profiles with $\sqrt{\psi} > 0.5$ are depicted in the insets.

So far, we have only considered the spatial transport of α particles. Without energy diffusion, the number of particles with high energy in the current simulation is larger than that in reality. Since particles with higher energy are more easily lost due to their larger orbital width, the number of lost particles is overestimated. In addition, helium ash is not included in the model, i.e., all α particles are regarded as energetic particles. During the Coulomb collision between EP and background plasma, the EP continuously loses energy, and finally transfers to helium ash. The diffusion coefficients of EP and ash are quite different. The energy-dependent mechanism can be neglected in current experimental devices, since the injected energy of NBI is only $O(10)$ keV. However, it will become significant for 3.5 MeV α particles in future fusion devices.

In summary, the α particle redistribution of the CFETR steady-state scenario is predicted by our improved CGM, which takes into account the fact that threshold evolution relieves the abnormally flat profile in the unstable AE region. The FOW effect adds an additional sink for EP loss. The simulation indicates that unstable AE enhances EP radial transport, pushing the particles outwards, so that the particles move into the loss cone and escape. Separate mechanisms only result in slight EP loss, but the combination of AE and FOW raises the loss to 6.6%. The lost fraction is still much lower than that measured in current experiments, benefitting from a well-separated unstable AE and loss cone region.

References

[1] Wan Y *et al.* 2017 *Nucl. Fusion* **57** 102009
[2] Zhuang G *et al.* 2019 *Nucl. Fusion* **59** 112010
[3] Chen W and Wang Z 2020 *Chin. Phys. Lett.* **37** 125001
[4] Meneghini O *et al.* 2015 *Nucl. Fusion* **55** 083008
[5] Lao L L *et al.* 1981 *Phys. Fluids* **24** 1431
[6] Van Zeeland M A *et al.* 2011 *Phys. Plasmas* **5** 056114
[7] Heidbrink W W *et al.* 2017 *Phys. Plasmas* **24** 056109
[8] Pace D C *et al.* 2011 *Nucl. Fusion* **51** 043012
[9] Todo Y, Berk H L and Breizman B N 2010 *Nucl. Fusion* **50** 084016
[10] Todo Y *et al.* 2014 *Nucl. Fusion* **54** 104012
[11] Bass E M and Waltz R E 2010 *Phys. Plasmas* **17** 112319
[12] Fu G and Van Dam J W 1989 *Phys. Fluids B: Plasma Phys.* **1** 1949
[13] He S, Waltz R E and Staebler G M 2017 *Phys. Plasmas* **24** 072305
[14] Bass E M and Waltz R E 2017 *Phys. Plasmas* **24** 122302
[15] Collins C S *et al.* 2017 *Nucl. Fusion* **57** 086005
[16] Candy J and Waltz R E 2003 *J. Comput. Phys.* **186** 545
[17] Waltz R E and Bass E M 2014 *Nucl. Fusion* **54** 104006
[18] Waltz R E *et al.* 2015 *Nucl. Fusion* **55** 123012
[19] He S and Waltz R E 2016 *Nucl. Fusion* **56** 056004
[20] Betti R and Freidberg J P 1992 *Phys. Fluids B: Plasma Phys.* **4** 1465
[21] Angioni C and Peeters A G 2008 *Phys. Plasmas* **15** 052307
[22] White R B and Chance M S 1984 *Phys. Fluids* **27** 2455
[23] Lao L L *et al.* 1985 *Nucl. Fusion* **25** 1611
[24] Cheng C Z and Chance M S 1987 *J. Comput. Phys.* **71** 124
[25] Estrada-Mila C, Candy J and Waltz R E 2006 *Phys. Plasmas* **13** 112303
[26] Van Zeeland M A *et al.* 2012 *Nucl. Fusion* **52** 094023
[27] Bass E M and Waltz R E 2020 *Nucl. Fusion* **60** 016032